

Evaluating Rotational Diffusion from Protein MD Simulations[†]

Vance Wong and David A. Case*

Department of Molecular Biology, The Scripps Research Institute, La Jolla, California 92037

Received: August 1, 2007; In Final Form: October 1, 2007

It is now feasible to carry out molecular dynamics simulations of proteins in water that are long compared to the overall tumbling of the molecule. Here, we examine rotational diffusion in four small, globular proteins (ubiquitin, binase, lysozyme, and fragment B3 of protein G) with the TIP3P, TIP4P/EW, and SPC/E water models, in simulations that are 6 to 60 times as long as the mean rotational tumbling time. We describe a method for extracting diffusion tensors from such simulations and compare the results to experimental values extracted from NMR relaxation measurements. The simulation results accurately follow a diffusion equation, even for spherical harmonic correlation functions with l as large as 8. However, the best-fit tensors are significantly different from experiment, especially for the commonly used TIP3P water model. Simulations that are 20 to 100 times longer than the rotational tumbling times are needed for good statistics. A number of residues exhibit internal motions on the nanosecond time scale, but in all cases examined here, a product of internal and overall time-correlation functions matches the total time-correlation function well.

1. Introduction

Macromolecules in aqueous solution undergo a variety of thermal motions. Their overall rotational tumbling is regulated by frequent collisions with light water molecules. For a nearly rigid molecule, this physical model should lead to diffusive rotational behavior, where the reorientation of a unit vector attached to the molecule undergoes a random walk on the surface of a sphere. If $c(\mathbf{n}, t)$ is the probability density for finding the vector pointing direction \mathbf{n} at time t , a spherical molecule should follow a simple diffusion equation:^{1,2}

$$\frac{\partial c(\mathbf{n}, t)}{\partial t} = D \nabla^2 c(\mathbf{n}, t) = -D_{\text{rot}} \hat{I}^2 c(\mathbf{n}, t) \quad (1)$$

Here \hat{I} is a (dimensionless) angular momentum operator. A nonspherical molecule will tumble more rapidly about some directions than about others, causing the diffusion constant D_{rot} to become a tensor:

$$\frac{\partial c(\Omega, t)}{\partial t} = - \sum_{ij} \hat{I}_i \cdot \mathbf{D}_{ij} \cdot \hat{I}_j c(\Omega, t) \quad (2)$$

Here Ω represents the Euler angles that specify the orientation of the macromolecule.

The most powerful way to measure macromolecular diffusion is by NMR relaxation, since it is very sensitive to both the overall tumbling frequency and its anisotropy.^{3,4} For a rigid molecule that rotates as a whole, the influence of molecular motion on spin transition rates is governed by components of a spectral density function, $j(\omega)$, which is the Fourier transform of a time-correlation function:

$$C_{lm}(\tau) = \left(\frac{4\pi}{2l+1} \right) \langle Y_{lm}^*(\mathbf{n}(0)) Y_{lm}(\mathbf{n}(\tau)) \rangle \quad (3)$$

For dipolar coupling, the unit vector \mathbf{n} lies along the vector

connecting the two spins, whereas for axial CSA tensors, it is the direction of unique principal component of the shielding tensor. The brackets in eq 3 indicate an average over all the molecules in the ensemble, and Y_{lm} is a spherical harmonic. For most aspects of NMR relaxation, the $l = 2$ terms are needed, but experiments such as dielectric relaxation depend on $l = 1$. If there is no preferred direction in space, as in isotropic solution or in a randomly oriented powder, the expression in eq 3 is independent of the subscript m , and we can average over the $2l + 1$ possible values using the spherical harmonic addition theorem. This gives

$$C_l(\tau) = \langle P_l[\mathbf{n}(0) \cdot \mathbf{n}(\tau)] \rangle \quad (4)$$

where $P_l(x)$ is a Legendre polynomial.

The analysis of NMR relaxation data typically assumes that the rotational motion of a compact and folded protein follows eq 2, so that the goal of the analysis is to determine the principal values and orientation of the diffusion tensor \mathbf{D} . Deviations from the behavior predicted for a single diffusion tensor are generally taken as evidence for internal motion (i.e., for nonrigid behavior), most commonly using a model-free formalism that assumes a statistical independence of internal and overall motion.^{5,6} While there is no question that this overall description is qualitatively correct for many well-folded proteins, quantitative analyses of NMR relaxation data increasingly face questions about the correctness of these assumptions. Does overall rotation follow diffusion theory (with a single tensor \mathbf{D}), or would it be more correct to adopt a model with a distribution of tensors or correlation times?^{5,7} Are typical internal motions of proteins uncorrelated with overall rotational motion, and can we approximate the full correlation function as a product of separate overall and internal functions? As proteins become more disordered (either in toto or as a result of floppy “tails”), how quickly do these standard models fail?

In principle, molecular dynamics simulations should have a lot to say about these questions, since they provide a very detailed (albeit approximate) description of macromolecular

[†] Part of the “Attila Szabo Festschrift”.

* Corresponding author.

TABLE 1: Self-Diffusion Constants for the Models of Water Used Here Where Data for TIP4P/EW Is from Ref 8, and Remaining Data Is from Ref 9

model	D^{298} , 10^{-9} m ² s ⁻¹
experiment	2.2
TIP3P	5.7
SPC/E	2.8
TIP4P/EW	2.3

structure and dynamics. To date, most studies along these lines have been devoted to the study of internal motions, since many of these operate at a short enough time scale (tens to hundreds of picoseconds) to be studied with current computers and computational techniques.^{6,10} One can learn some information about global motion by extrapolations from even short simulations,¹¹ but the longer time scales now available are expected to yield more reliable information. Furthermore, many popular water models (such as TIP3P) predict self-diffusion constants and viscosities that are far from experiment (see Table 1), so that one would not expect good results for rotational or translation diffusion of macromolecules dissolved in such solvents. Now that simulations that are many times longer than rotational diffusion times are feasible and simple water models are available with better diffusional properties, an examination of rotational motion and its connection to internal motion should yield interesting results. Here, we report simulations of 100–200 ns on 4 small proteins and examine the extent to which diffusional models match the dynamics data and the statistical independence of overall and internal motion. We consider how long simulations need to be to provide statistically reliable results, whether the simulated motion is indeed diffusive, and how the best-fit tensors compare to fits to experimental data.

2. Theory and Numerical Methods

2.1. Basics of Rotational Diffusion. For isotropic diffusional motion, solutions to eq 1 are easily computed for any value of l , and the correlation functions are single exponentials:²

$$C_l(\tau) = \exp[-l(l+1)D_{\text{rot}}\tau] \quad (5)$$

Things are more complex for anisotropic molecules, even though the general solution of the anisotropic rigid body diffusion problem has been known for many years.¹ It is a straightforward but algebraically complex matter to compute the time correlation function for a vector fixed to the rigid body using the Green's function of the rotational diffusion operator.^{12,13} The same result has been obtained without direct use of the diffusion operator eigenfunctions.¹⁴ For $l = 1$, the correlation function generally will be written as a sum of three exponentials:¹²

$$C_1(\tau) = \sin^2 \theta \cos^2 \varphi \exp[-(D_y + D_z)\tau] + \cos^2 \theta \exp[-(D_x + D_y)\tau] + \sin^2 \theta \sin^2 \varphi \exp[-(D_x + D_z)\tau] \quad (6)$$

Here, the polar angles give the orientation of n in the principal axis frame of the diffusion tensor. Rank 2 correlation functions have five exponentials that have been written down in many places.^{2,14–17} For simplicity, we show here results for a symmetric top (where $D_x = D_y$), which has three exponential terms; numerical calculations, however, were done using the fully anisotropic expression.¹⁷

$$C_2(\tau) = \frac{1}{4} \{ (3 \cos^2 \theta - 1)^2 \exp[-6D_x\tau] + 12 \cos^2 \theta \sin^2 \theta \exp[-(5D_x + D_z)\tau] + 3 \sin^4 \theta \exp[-(2D_x + 4D_z)\tau] \} \quad (7)$$

Hence, for anisotropic rotation, the simple dependence of the decay times on $l(l+1)$ seen in eq 5 no longer holds, although it is still on average valid to first order in the anisotropy (see eq 11 below).

2.2. Fitting the Diffusion Tensor: Singular Value Decomposition Procedure. In order to see how well correlation functions from MD simulations match diffusional behavior, we need to have a procedure for determining the optimal tensor. Here, we use a procedure that was developed for the analysis of NMR relaxation data,^{18–20} and which is well-suited for adaptation to the analysis of MD simulations. Although these correlation function decays are expected to be multiexponential, the proteins considered here have relatively small anisotropies, and it is not realistic to try to extract multiple decay times from the overall curves. Instead, we consider the average (or “effective”) correlation time for a particular vector, \mathbf{n} (e.g., a backbone N–H bond vector or a randomly chosen direction in the molecular frame), which can be defined as

$$\tau_l(\mathbf{n}) = \int_0^\infty d\tau \langle P_l[\mathbf{n}(0) \cdot \mathbf{n}(\tau)] \rangle \quad (8)$$

where

$$\langle P_l[\mathbf{n}(0) \cdot \mathbf{n}(\tau)] \rangle = \lim_{T \rightarrow \infty} \frac{1}{T} \int_0^T P_l[\mathbf{n}(t) \cdot \mathbf{n}(t - \tau)] dt \quad (9)$$

is the usual time correlation function of a Legendre polynomial of order l . Note that $\tau(\mathbf{n}) \simeq j(0)$, the zero-frequency component of the corresponding spectral density function. This correlation time is related to a “local” or effective diffusion constant by:

$$d_{\text{loc}}(\mathbf{n}, l) \equiv \frac{1}{l(l+1)\tau_l(\mathbf{n})} \quad (10)$$

Assuming that the rotational motion of \mathbf{n} can be described by a Brownian motion model, it can be shown that, for diffusion tensors with small anisotropy, $d_{\text{loc}}(\mathbf{n}, l)$ may be written as a quadratic function in \mathbf{n} :^{18–20}

$$d_{\text{loc}}(\mathbf{n}, l) = \mathbf{n}^T \cdot \mathbf{Q} \cdot \mathbf{n} \quad (11)$$

where

$$\mathbf{Q} = \frac{3D_{\text{av}}\mathbf{I} - \mathbf{D}}{2} \quad (12)$$

(This can be directly established by inserting eq 6 or eq 7 into eq 8, expanding in powers of $D_x - D_z$, and simplifying terms.) The tensors \mathbf{D} and \mathbf{Q} encode equivalent but complementary information: whereas $1/[l(l+1)D_{kk}]$ is the time constant for diffusion about the k th axis (in the principal axis frame of the diffusion tensor,) $1/[l(l+1)Q_{kk}]$ gives the time constant for the rotational diffusion of the k th axis.¹⁹ Since the right-hand side of eq 11 is independent of l , d_{loc} should also be independent of l when the motion is well-characterized as rotational diffusion of \mathbf{n} . Indeed, one test of whether a diffusion model fits the MD data is to examine the dependence of d_{loc} (or, equivalently τ_l) on l .^{2,11}

In NMR experiments, d_{loc} (or $j(0)$) is generated from data that report on the spectral density function of rank 2 interactions

(e.g., dipolar and CSA) so that $d_{\text{loc}}(\mathbf{n}, 2) = 1/6\tau_2(\mathbf{n})$ is taken to be the relevant local diffusion constant. Here, \mathbf{n} is often a backbone N–H bond vector, and $d_{\text{loc}}(\mathbf{n}, 2)$ is computed as a function of $R_2(\mathbf{n})/R_1(\mathbf{n})$ (or related quantities, such as $(2R_2 - R_1)/R_1$), where R_1 and R_2 are longitudinal and transverse relaxation rates.^{20,21} (Various analysis procedures can be used to minimize the effects of internal motion.) From MD simulations, we can only compute reliable values of $C_l(\tau)$ for relatively short times τ ; our method to obtain $d_{\text{loc}}(\mathbf{n}, l)$ is described in section 2.3, below. In this way, the local diffusion constants become a key intermediate quantity that can be estimated from both NMR experiments and from simulations; in this respect, they play much the same role here as the model-free parameters S^2 and τ_e play in the analysis of internal motions by MD.

Equation 11 can also be written in the form

$$d_{\text{loc}}(\mathbf{n}, l) = \mathbf{A}^T(\mathbf{n})\mathbf{Q} \quad (13)$$

where $\mathbf{A}^T(\mathbf{n}) = [x^2, y^2, z^2, 2xy, 2yz, 2xz]$, and $\mathbf{Q}^T = [Q_{xx}, Q_{yy}, Q_{zz}, Q_{xy}, Q_{yz}, Q_{xz}]$. Here $x, y,$ and z are Cartesian coordinates of the vector \mathbf{n} in the molecular coordinate system. Data from N vectors may then be used to fit the diffusion tensor by constructing a column vector whose components are $d_{\text{loc}}(\mathbf{n}, l)$, whereupon eq 13 becomes a matrix equation whose left-hand side is a column vector of length N , and $\mathbf{A}^T(\mathbf{n})$ is an N -by-6 matrix. This may be solved for \mathbf{Q} (and therefore \mathbf{D}) using singular value decomposition (SVD).²² The resulting \mathbf{D} is then diagonalized to yield its principal components and principal axes. Such tensors are often characterized by their isotropic diffusion constants $D_{\text{av}} \equiv (D_x + D_y + D_z)/3$ and their anisotropy (Δ) and rhombicity (δ), defined as:²³

$$\Delta = \frac{2D_z}{D_x + D_y} \quad (14)$$

$$\delta = \frac{\frac{3}{2}(D_y - D_x)}{\left[D_z - \frac{1}{2}(D_x + D_y)\right]} \quad (15)$$

Here, $D_x \leq D_y \leq D_z$ are principal values of the diffusion tensor.

Equation 13 is only strictly valid in the limit of small anisotropy in \mathbf{D} , but we expect the errors due to this assumption to be moderate. In particular, it has been shown with simulated data assuming an axially symmetric tensor, that fractional errors in D_{av} and D_{\parallel}/D_{\perp} are no greater than a few percent for tensors with anisotropies in the range we consider here.¹⁹ This should be sufficient for analyses of the accuracy of molecular mechanics potentials and the adequacy of the sampling provided by trajectory lengths currently accessible by MD simulation.

We have selected the directions \mathbf{n} randomly from directions uniformly distributed on the unit sphere; for the calculations reported here, 1000 such directions were used. The time-correlations functions for these vectors were generated by applying the orthogonal matrix that rotates a reference structure (the average over the trajectory) into the structure at a given time in the MD simulation, that is, the rotation matrix determined by the usual root mean squared deviation (rms) fitting procedure. Though rms fitting instantaneous configurations of the trajectory to a reference structure is a well-established method for removing rotational and translation motion from the analysis of internal motion,²⁴ there is continuing debate about which set of atoms provides the best results for this purpose.^{25–28} Tests using other choices (such as backbone atoms in regular secondary structure) gave results nearly

identical to those reported here. (This lack of sensitivity to the rms fitting scheme might not hold for floppier proteins.)

2.3. Determining Local Diffusion Constants from Simulation Data. From the simulation data, the correlation time is found by integrating the time correlation function as shown in eq 8. While the correlation functions may be easily computed from the trajectories, statistical errors due to finite trajectory length limit the useful data to short delay times τ .^{29,30} In order to estimate the full integral in eq 8, we resorted to an iterative procedure for estimating τ_l . We define the function $F(\mathbf{n}, \tau_f)$:

$$F_l(\mathbf{n}, \tau_f) = \int_0^{\tau_f} dt \langle P_l[\mathbf{n}(t) \cdot \mathbf{n}(t - \tau)] \rangle \quad (16)$$

In practice, we simply used the Romberg integrator²² to numerically integrate the correlation functions. If $\langle P \rangle$ were an exponentially decaying function of time delay with decay constant $\tau(\mathbf{n})$, we would have

$$F_l(\mathbf{n}, \tau_f) = \tau_l(\mathbf{n}) \{1 - \exp[-\tau_f/\tau_l(\mathbf{n})]\} \quad (17)$$

This can be rearranged to give the following equation, which is to be solved iteratively until self-consistency is achieved between right- and left-hand sides:

$$\tau_l(\mathbf{n}) \equiv \frac{1}{l(l+1)d_{\text{loc}}(\mathbf{n})} = \frac{F_l(\mathbf{n}, \tau_f)}{1 - \exp[-\tau_f/\tau_l(\mathbf{n})]} \quad (18)$$

The single time-scale assumption is an oversimplification, given that anisotropic diffusion is known to yield multiexponentially decaying correlation functions.^{12–14} We do not expect this to be the limiting factor in the accuracy of our method, given that time constants for the exponentials should differ by less than a factor of 2. However, one must still address the question of what the optimum value of τ_f is, if it exists at all. As we show below, for most of our data, the results for D_{av} are nearly independent of the integration limit τ_f which is less true for quantities like Δ and δ .

2.4. Details of the Simulations. We carried out molecular dynamics simulations on the four small, monomeric proteins shown in Figure 1. All calculations used the Amber 9 simulation package³³ and the “ff99SB” protein force field.^{34,35} The water model used was either SPC/E³⁶ or TIP4P/EW;⁸ we also report results for published simulations³⁵ of ubiquitin and lysozyme using the TIP3P water model.

For all simulations, the crystal structure was immersed in a truncated octahedral box of water, with a buffer of 12 Å between the protein atoms and the edge of the box, so that there is a minimum of 24 Å between any protein atom and an atom of an image in a neighboring unit cell. Sodium or chloride ions were added to neutralize the net charge. Details about the starting structures and number of solvent molecules are given in Table 2. The system was initially equilibrated to 300 K and 1 atm pressure for 0.2 ns, with 1 kcal/mol restraints on all protein atoms, to keep them from moving away from their starting positions. This was followed by an additional 0.1 ns equilibration with 0.1 kcal/mol restraints, followed by a 1 ns NVE simulation with no restraints. The “production” phase of simulation then followed, in the NVE ensemble, for 100 ns (or 200 ns for GB3 + SPC/E). The NVE ensemble was used because we are interested here in dynamical effects, which would be perturbed by use of a thermostat. These systems are large enough (with 15 000 to 30 000 atoms) that the microcanonical and canonical ensembles are nearly the same. The calculations used a 1 fs integration time step and an 8 Å direct-space cutoff for Lennard-

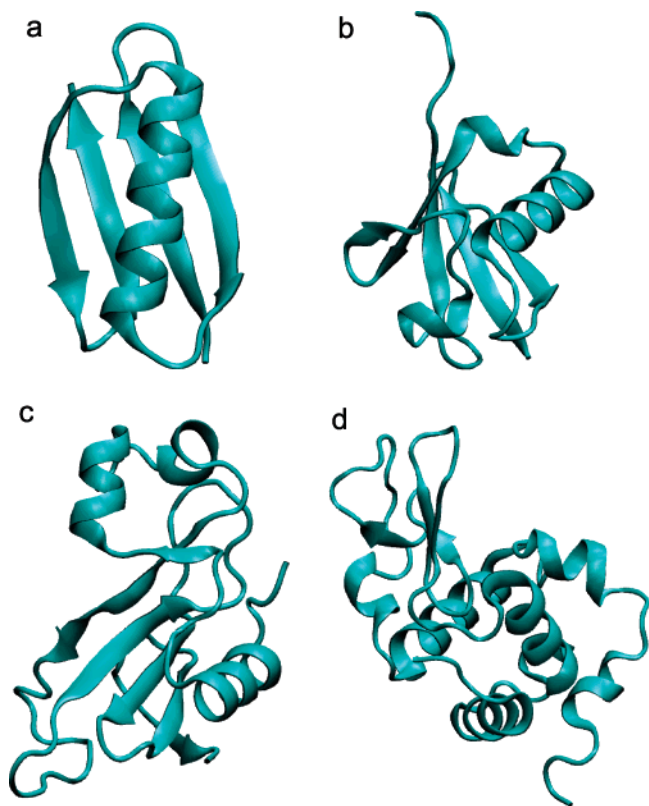


Figure 1. Backbone cartoons for (a) GB3,³¹ (b) ubiquitin, (c) binase,³² and (d) hen egg-white lysozyme.

TABLE 2: Details of the Simulations

protein	PDB	# amino acids	water model	# waters	length, ns
GB3	1p7e	56	SPC/E	4473	200
			TIP4P/EW	4443	100
ubiquitin	1ubq	76	SPC/E	5955	100
			TIP4P/EW	5895	100
binase	<i>a</i>	109	SPC/E	9158	100
lysozyme	132l	129	SPC/E	10741	100

^a X-ray dataset for binase kindly provided by G. Dodson (University of York); resolution of 1.8 Å.

Jones and electrostatic interactions. Long-range electrostatic effects were described with a PME procedure using default parameters. Although the simulations should be following Newtonian dynamics at constant total energy, there is a small energy drift, primarily due to noise caused by neglect of Lennard-Jones interactions beyond the cutoff but also partly due to discretization errors in the PME procedure. As a result, the average temperature increases by about 0.5 K over the 100 ns of simulation time. This should have only a small effect on the behavior reported here.

Trajectory snapshots were collected every 2 ps, and correlation functions were calculated using the *ptraj* module of Amber, which was modified to use higher values of l in eq 9. Overall motion was monitored by keeping track of the rotation matrixes needed for an rms superposition of C α atoms (excluding the first two and last two residues) to the average structure. (For ubiquitin, we used C α atoms of residues 3–71 for the superposition.) The structures moved only small amounts (less than 1 Å, except for binase) from their starting points, as indicated in Figure 2. Other results from these simulations, including an analysis of internal motions and hydrogen-bonding, will be presented elsewhere.

3. Results and Discussion

3.1. Uncertainties in Correlation Functions and Diffusion Tensors. As mentioned above, sampling a finite length trajectory gives rise to nonzero variance or uncertainty in time correlation functions. This is a likely source of nonexponential decays in cases where the trajectory length T does not exceed the true decay time τ by nearly 3 orders of magnitude.³⁰ The trajectories surveyed in this study fall in the range $10 < T/\tau < 60$ for $l = 2$. Therefore, any apparent nonexponential character of the correlation functions could easily be a consequence of finite trajectory length. The variance of a Gaussian process may be estimated using the Bartlett formula,^{37,38} which when applied to an isotropic rotational diffusion process yields^{29,30}

$$\sigma(j) = \left\{ \frac{1}{T_s} [1 - (1 + 2j_s) \exp(-2j_s)] \right\}^{1/2} \quad (19)$$

Here, j is the $(j - 1)$ th data point in the time series, $T_s = T/\tau$ is the scaled trajectory length, and $j_s \equiv j/\tau$ is the scaled delay. Figure 3 (left) shows a single $l = 2$ correlation function generated from a member of the random initial vector set for the GB3 (ff99sb + SPC/E) trajectory, together with estimates of variance computed using eq 19. The expected variance is small for short delays but becomes larger as $C(\tau)$ decays. For the parameters of the figure, the expected uncertainty in $C(\tau)$ is about 0.06 at $j_s = 1/2$ and grows to 0.09 by the time $j_s = 1$, that is, at a delay time equal to the rotational correlation time; the latter value corresponds to a 23% relative uncertainty, which clearly has a significant impact on the ability to estimate the rate at which the true correlation function decays.

An alternative scheme for characterizing the uncertainty in the correlation function, which would not assume a Gaussian process, might be based on a division of a trajectory into shorter segments. Correlation functions computed for halves and quarters for our trajectory are also shown in Figure 3. At a fixed delay, the correlation functions from the segments provide a distribution of values for the correlation function. The correlation functions from the shorter trajectories cluster about the mean somewhat more tightly than what would be predicted from eq 19, suggesting that the actual reproducibility of results is a little better than predicted by the statistical theory. A less well-behaved result is shown at the right of Figure 3. Here, the deviations of the slopes in the subsections of the trajectory deviate from the full run at shorter delay times (as early as 1 ns), and the spread in results is worse at larger times as well. There is also a noticeable nonexponential character to the correlation function for the full trajectory. Even this result, which is among the worst we saw, could be accommodated by the statistical error bars indicated in the left-hand panel.

Any uncertainties in the slopes in plots like that of Figure 3 will propagate into uncertainties in the fitted diffusion tensors. A simple approach to characterizing this error propagation can be made by again analyzing shorter segments and by varying the integration time τ_f in eq 18. Results for D_{av} are shown in Figure 4. For the full trajectories (shown in blue), the results are nearly independent of τ_f : for GB3, for example, the fitted value varies only between 0.070 and 0.071 ns⁻¹ as τ_f ranges from 0.1 to 5 ns. Similar behavior is seen for lysozyme and binase, but the dependence on τ_f is much stronger for ubiquitin, where the estimate of D_{av} varies by about 20%. Nearly identical behavior is seen for the ubiquitin + TIP4P/EW simulation (data not shown). We do not know why ubiquitin is different from the other three proteins in this respect; it may be due to the presence of the C-terminal tail (see Figure 1), which could lead

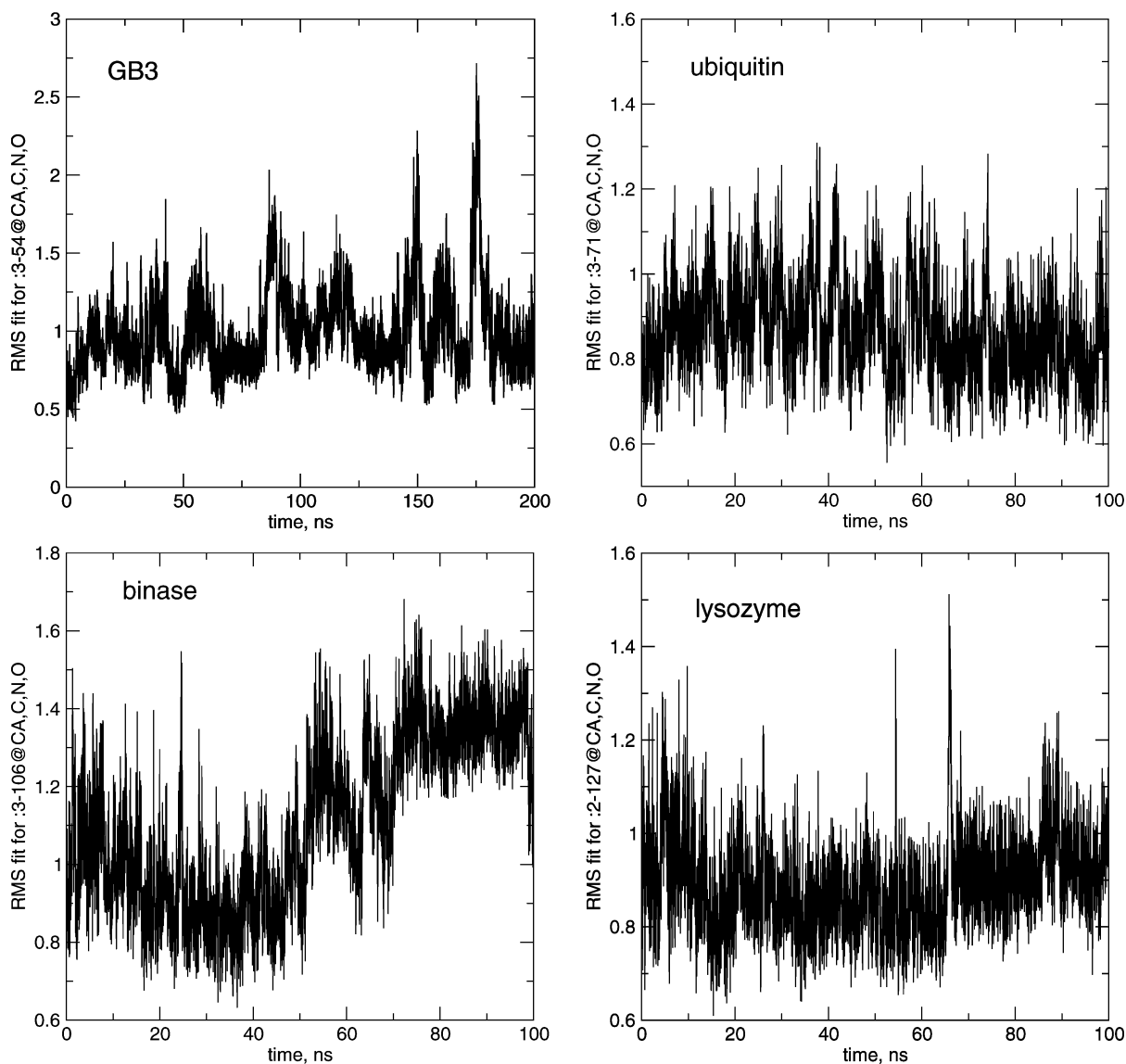


Figure 2. Root mean square superpositions to the starting structures for the SPC/E simulations.

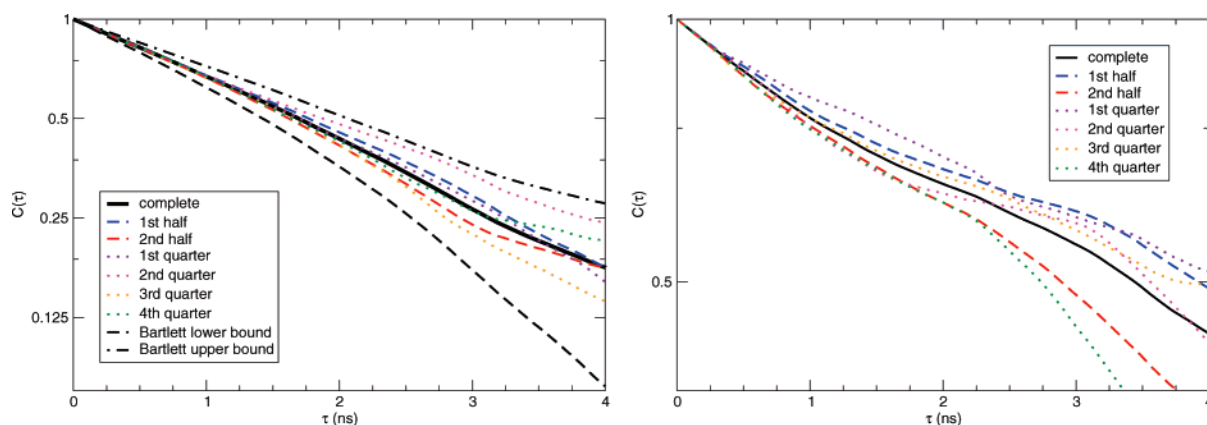


Figure 3. Left: semilog plot of $C_2(\tau)$ vs delay time, for a randomly chosen direction in the GB3 + SPC/E simulation (solid black line), with values computed from pieces of the trajectory in colored lines. Dashed lines are the error bounds from eq 19, using $T = 200$ ns, $\tau = 2.5$ ns, so that $T_s = 80$. Right: same, for a randomly chosen vector in the ubiquitin + SPC/E simulation.

to breakdown of the single-diffusion-tensor hypothesis. Further studies on this point are ongoing.

Figure 4 indicates that the precision with which even the average diffusion constant can be determined degrades rapidly with shorter simulations. For example, the four quarters of the GB3 trajectory (50 ns each) are best fit by values of D_{av} that

range from 0.06 to 0.08 ns⁻¹ at $\tau_f = 2$ ns. Generally, the results at shorter integration times τ_f match the full trajectory better than those at longer integration times.

One might expect more difficulty in determining the anisotropy or rhombicity of a diffusion tensor, since these quantities depend on the details of the motion rather than just on the

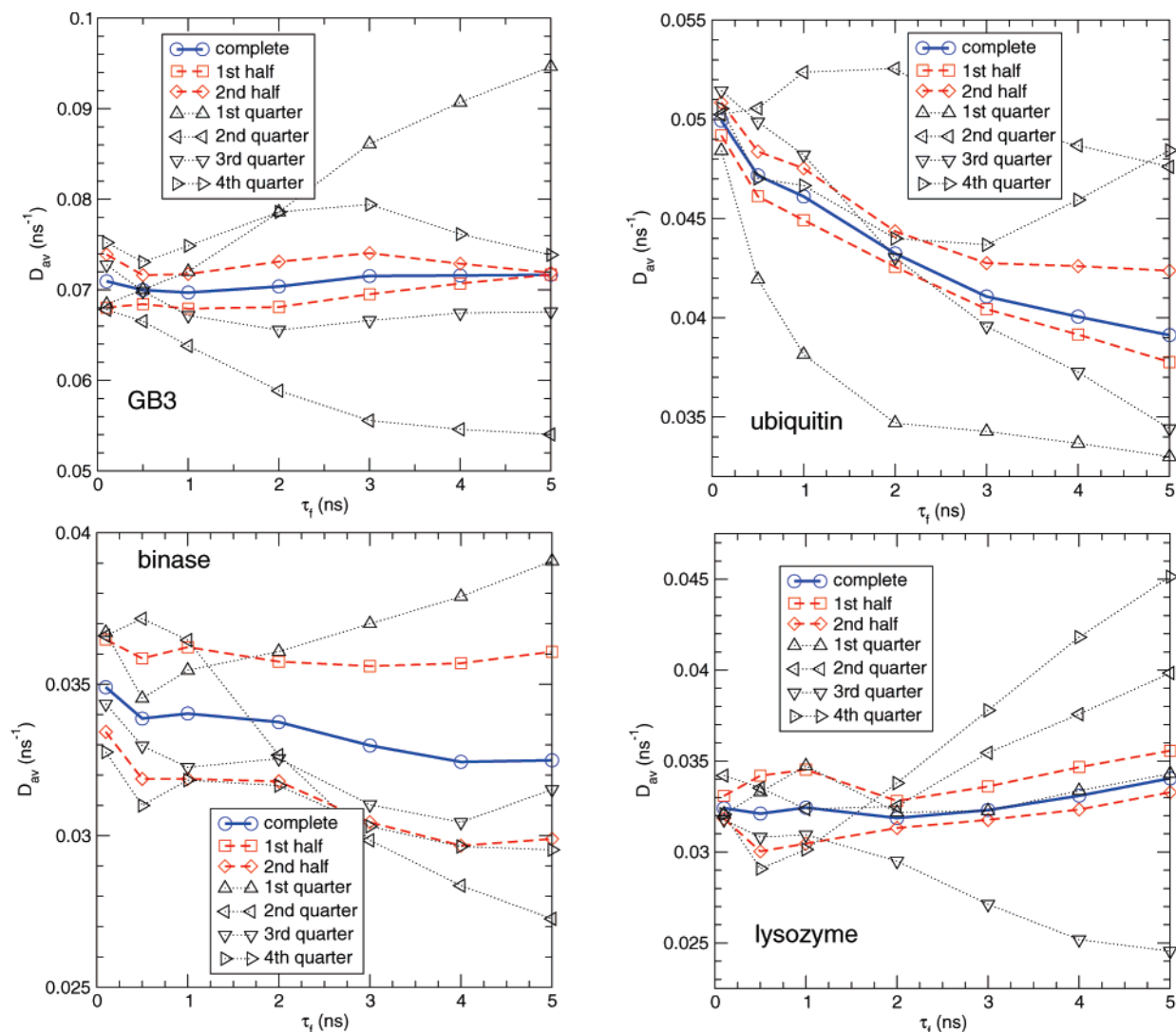


Figure 4. Dependence of D_{av} on the integration time τ_f . Upper left, GB3; upper right, binase; lower left, lysozyme; lower right, ubiquitin (all with SPC/E).

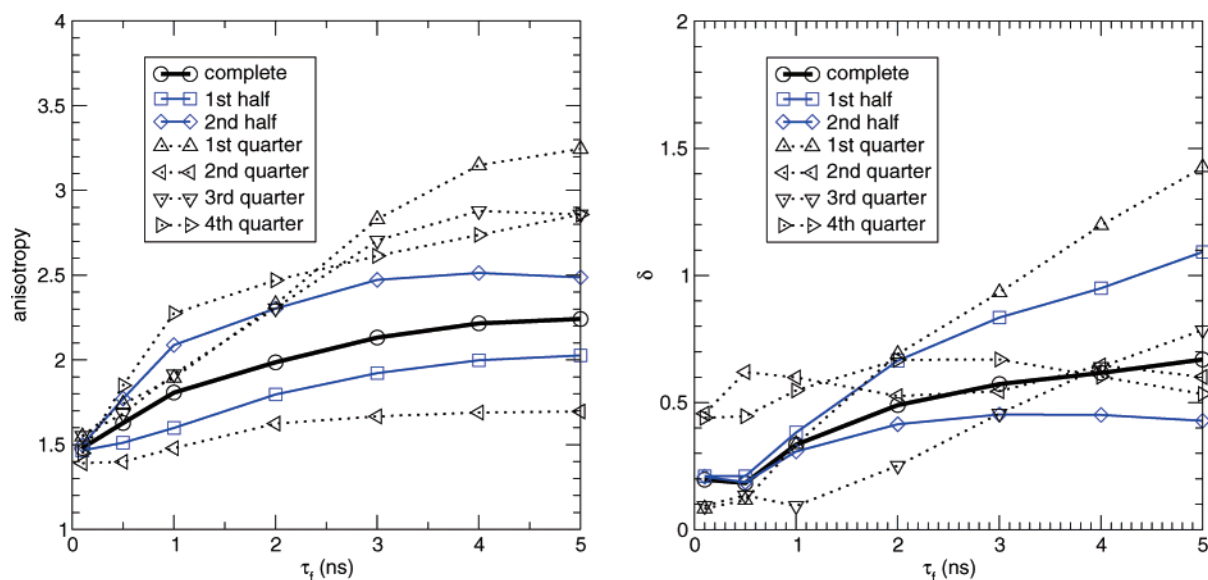


Figure 5. Dependence of Δ (left, eq 14) and δ (right, eq 15) on integration time τ_f , for the GB3 + SPC/E trajectory. average rotational tumbling time. This expectation is borne out in Figure 5, which shows Δ and δ of the fitted tensors as a function of τ_f for the GB3 simulation. Even for the full 200 ns simulation, the best-fit anisotropy Δ varies from 1.5 to 2 as a

function of τ_f , and the rhombicity parameter δ ranges from 0.2 to 0.5. Shorter segments of the trajectories show even larger variations. As with D_{av} , the most consistent results appear to come from the use of short times for τ_f , but it seems clear that

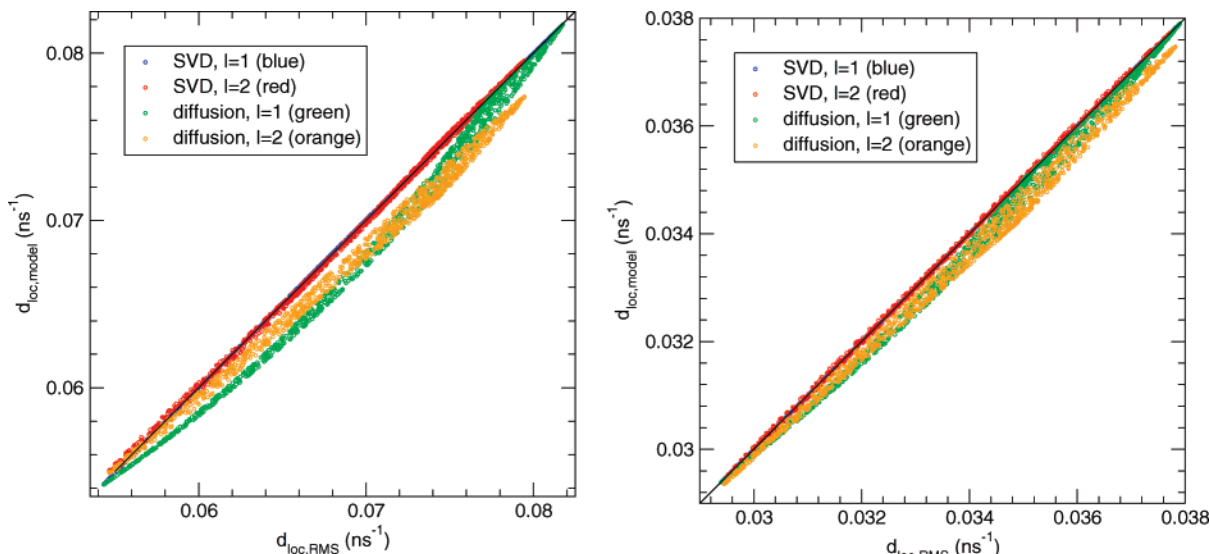


Figure 6. Comparison of d_{loc} values derived from the trajectory (eq 18, with $\tau_f = 1$ ns) with values from diffusion theory, using either low-anisotropy limit (eq 11) or the fully anisotropic theory (eq 6 or 7) both using the SVD-fit diffusion tensor. Left, GB3 + SPC/E; right, binase + SPC/E.

TABLE 3: Calculated ($l = 2$) Diffusion Tensors, Using $\tau_f = 1$ ns

protein (force field)	D_{av} (ns^{-1})	Δ	δ	r^2 (eq 13)	r^2 (eq 7)
GB3 (ff99sb + SPC/E)	0.070	1.81	0.33	0.9992	0.9955
GB3 (ff99sb + TIP4P/EW)	0.060	1.58	0.45	0.9998	0.9960
GB3 (experiment ^d)	0.055	1.43	0.37		
ubiquitin (ff99sb + TIP3P ^e)	0.109	2.32	0.27	0.9995	0.9912
ubiquitin (ff99sb + SPC/E)	0.046	1.18	1.08	0.9985	0.9973
ubiquitin (ff99sb + TIP4P/EW)	0.047	1.39	0.72	0.9998	0.9963
ubiquitin (experiment ^b)	0.041	1.16	0.268		
binase (ff99sb + SPC/E)	0.034	1.47	0.64	0.9997	0.9956
binase (experiment ^c)	0.028	N/A	N/A		
lysozyme (ff99sb + TIP3P ^e)	0.064	1.69	0.56	0.9997	0.9924
lysozyme (ff99sb + SPC/E)	0.032	1.31	1.24	0.9999	0.9971
lysozyme (experiment ^d)	0.024	N/A	N/A		

^a Fitted to asymmetric top model; corrected from 297 K and 9% D₂O; from ref 23. ^b Fitted to asymmetric top model; from ref 39. ^c Corrected from 303 K; from ref 40. ^d Corrected from 308 K and 5% D₂O; from ref 41. ^e Simulation described in ref 35.

even longer sampling may be required to determine the extent of anisotropy of the diffusion tensor with good precision.

3.2. Do the Simulations Exhibit Diffusive Motion? While it is always possible to find the best-fit diffusion tensor from the correlation functions of a reorienting molecule, the rotational dynamics need not be diffusive. For example, the rotation of small molecules in solution can be much more inertial in character than one would ordinarily expect for a macromolecule.² A more relevant scenario to protein dynamics would be instances where a single diffusion tensor cannot describe global tumbling because of conformational transitions that change the shape of the protein.

With this in mind, we characterize here the degree to which both eq 13 and the full diffusion theory (parametrized using the best fit tensor) are able to reproduce the local diffusion constants from eq 18. Figure 6 shows scatter plots comparing the MD results with diffusion theory. For both molecules (and for others not shown), there are some deviations from the perfect $y = x$ line, especially for the full diffusion tensor model. In spite of these minor deviations, it is clear from Figure 6 that fits of the MD to a diffusion model are actually quite accurate for these proteins. Table 3 shows that the squared correlation coefficients (r^2) are all larger than 0.99 when comparing the MD and diffusion model results for d_{loc} .

A hallmark of diffusion theory is that time correlation functions decay as $1/[l(l+1)D_{av}]$ in the limit of small anisotropy. In Figure 7, we present histograms of the ratio $d_{loc}(l=2)/d_{loc}(l=1)$ for 1000 random directions for the GB3 and ubiquitin simulations. Equation 11 implies that this ratio, for diffusional motion, must be equal to 1 in the limit of small anisotropy. Small anisotropy is not assumed in the diffusion results in Figure 7, so that some deviations from unity are expected. For both the full diffusion theory and the MD simulations, there are indeed small deviations from unity, up to 4% for GB3 ($l=2$) and up to about 0.4% for the more spherical ubiquitin. The magnitudes of the deviations from unity are roughly the same for the simulation as for diffusion theory, indicating that the diffusion model is a rather accurate representation of the simulation results.

An extension of this analysis to higher values of l is given in Figure 8. This shows that D_{av} changes by only a few percent as l varies from 1 to 8 and that again there is a weak dependence on τ_f . The fitted anisotropy parameter Δ is a stronger function of both l and τ_f , in agreement with the results noted above. This independence of l has been noted in earlier MD studies of rotational diffusion.¹¹

3.3. Comparison to Experiment. In Table 3, we present a comparison of experimentally determined D_{av} , Δ , and δ with

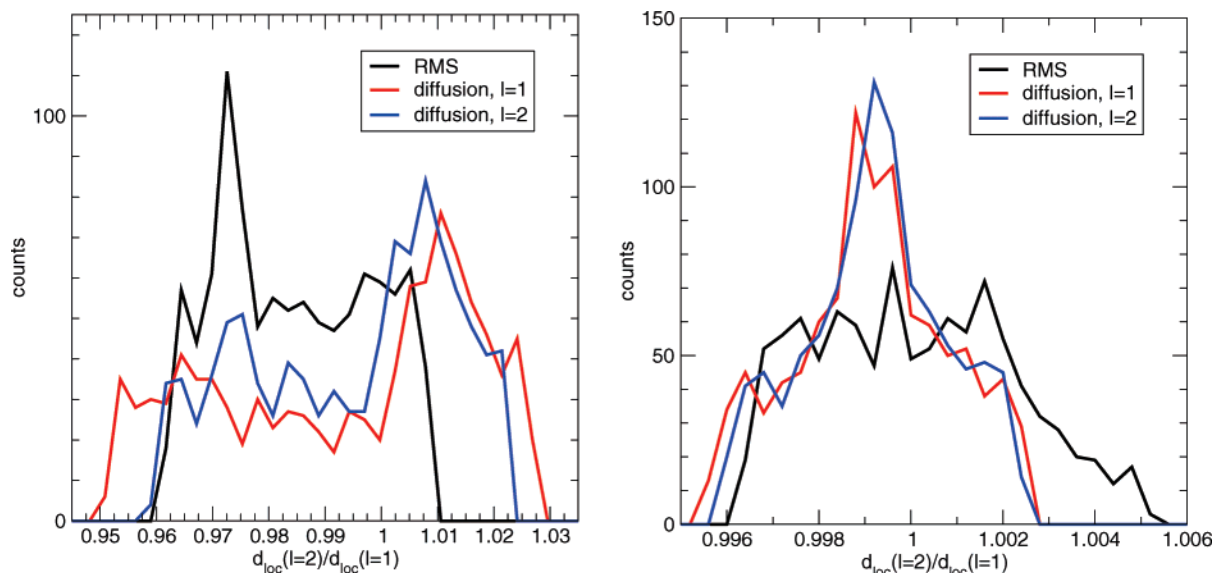


Figure 7. Histograms of $d_{\text{loc}}(l=2)/d_{\text{loc}}(l=1)$ for GB3 + SPC/E (left) and ubiquitin + SPC/E (right). Black lines show results from the simulations (using τ_f of 1 ns); red lines use eqs 6 and 7 and the diffusion tensor that best-fits the MD for $l=1$; blue lines use the best-fit tensor for the MD $l=2$ data.

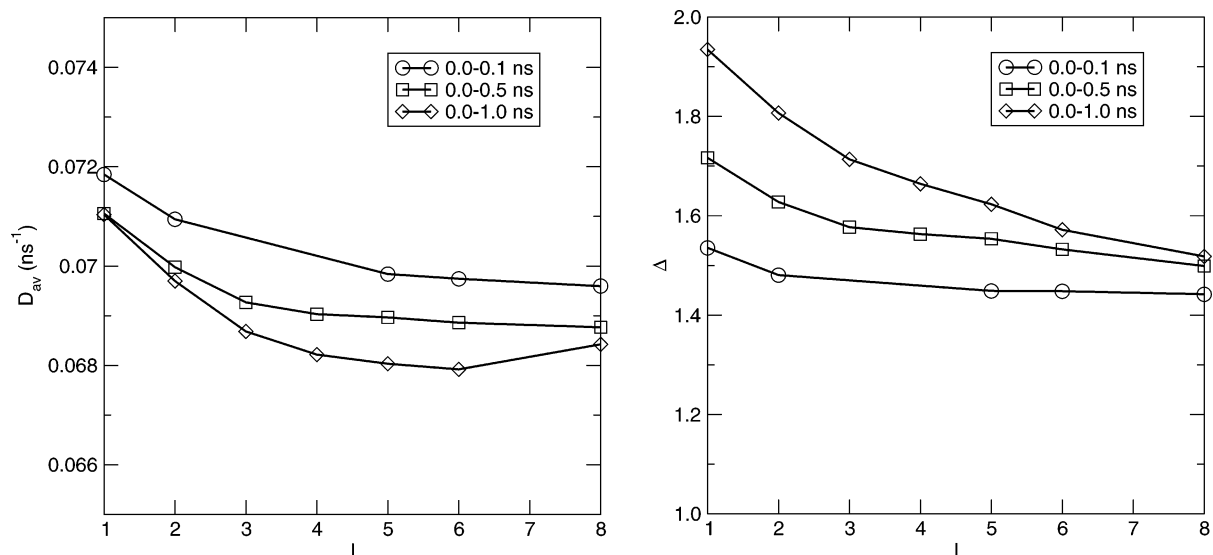


Figure 8. Dependence of D_{av} (left) or Δ (right) on the integration time and on the value of l for the GB3 + SPC/E simulation.

results obtained from the MD simulations. Experimental results were adjusted for temperature and D_2O content to standard conditions (pure H_2O at 300 K). Adjustments were based on the Stokes–Einstein relation

$$\tau = \frac{4\pi\eta r^3}{3kT} \quad (20)$$

implying

$$D'_{\text{av}} = D_{\text{av}} \frac{T'}{T} \frac{\eta}{\eta'} \quad (21)$$

Here, τ is the correlation time, η is the solvent viscosity, r is the molecule (assumed spherical) radius, at temperature T . The temperature dependence of water viscosity was taken from standard tables.⁴² The presence of D_2O was accounted for by assuming that $\eta_{\text{D}_2\text{O}}(T) = 1.23\eta_{\text{H}_2\text{O}}(T)$, giving

$$\eta(T) = \eta_{\text{H}_2\text{O}}(T)(1.23f_{\text{D}_2\text{O}} + f_{\text{H}_2\text{O}}) \quad (22)$$

Aside from the TIP3P trajectories, the simulation values of D_{av} are 10 to 30% larger than their experimental counterparts, as might be expected from the self-diffusion constants given in Table 1. Whereas D_{av} for GB3 in SPC/E water is noticeably larger than for GB3 in TIP4P/EW water, the corresponding results for ubiquitin are remarkably close to one another. This is apparent in Figure 9, where we present simulation and experimental D_{av} as a function of inverse molecular weight. Error bars in Figure 9 were obtained by taking the larger of the difference between the maximum or minimum and average D_{av} for the complete trajectories integrated over the delay intervals shown in Figure 4. Whereas experimental results obey the Stokes–Einstein relation (eq 20), which states that the diffusion tensors should be inversely proportional to volume (and hence to molecular weight, since the densities vary by less than 1% in these simulations), the SPC/E trajectories deviate from this expected behavior. However, with only four points, it is hard to know how much to make of this.

Figure 10 shows d_{loc} as a function of residue for two GB3 simulations (both with $\tau_f = 1.0$ ns) and for experiment. The

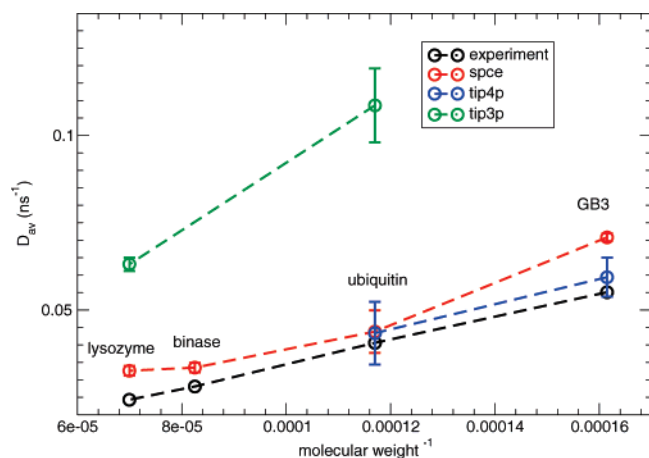


Figure 9. Calculated or experimental values of D_{av} , plotted against inverse molecular weight. Experimental values have been adjust to 300 K and pure H_2O , as described in the test.

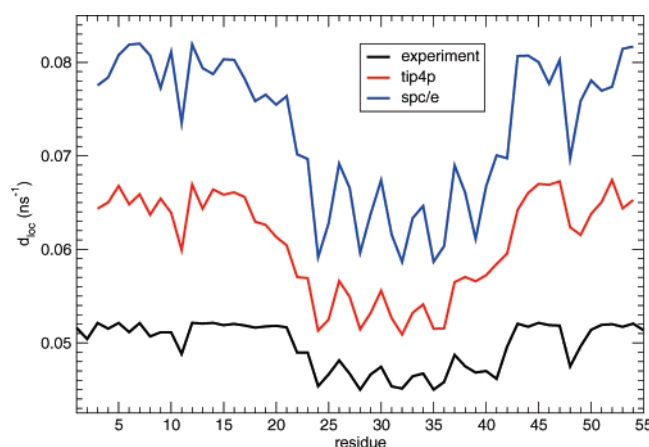


Figure 10. Local diffusion constants, from eq 18 and $\tau_f = 1$ ns, as a function of residue number, for GB3; experimental values are from ref 23.

simulation results are obtained from integration of $C_{rot}(\tau)$ generated by backbone NH bonds, whereas the experimental data were determined as described by Hall and Fushman.²³ The “comb-like” structure (between residues 23 and 39) in the d_{loc} data for GB3 (ff99sb + SPC/E) is generally characterized by slower diffusion than the remainder of the protein. Previous work has established that this is due to alignment of NH bonds within the central helix along the helix axis, which is also roughly parallel to the diffusion tensor axis of symmetry,²³ as can be seen in Figure 1. Overall, the shapes of the three curves are in good agreement with one another, but the degree of contrast between the central α -helix (residues 25–35) and the surrounding β -sheets is greater in the simulations than the experiments. (The increased anisotropy in the top two traces in Figure 10, compared with the bottom trace, is maintained if the trajectory is broken into halves or quarters.) This shows that the key qualitative features of the shape of the diffusion tensor are reproduced in the simulation. As expected from Figure 9, d_{loc} are largest for the simulation in SPC/E water and smallest for the experiment.

3.4 Factorization into Internal and Overall Correlation Functions. The extraction of a rotational diffusion tensor from MD simulation (or from experimental relaxation data) assumes that separation (in a statistical sense) of global tumbling and internal motion can be achieved. In terms of the time

correlation functions of interest in NMR relaxation, this can be expressed⁵

$$\langle P_l[n^{LF}(0) \cdot n^{LF}(t)] \rangle \approx \frac{4\pi}{2l+1} \sum_{m=-l}^l \sum_{n,n'=-l}^l \langle D_{mn}^l * (\Omega_0) D_{mn'}^l (\Omega) Y_{ln}^* (n_0^{MF}) Y_{ln'}(n^{MF}) \rangle \quad (23)$$

In eq 23, the reorientation of the protein is described by the Ω terms, whereas the motion of a particular vector (e.g., a backbone amide N–H vector) in the molecular frame is described by the terms involving n^{MF} . A physical uncoupling of overall and internal motions does not necessarily imply factorization of the global and internal motion correlation functions:

$$\langle P_l[n^{LF}(0) \cdot n^{LF}(t)] \rangle \approx C_{rot}(t) C_{int}(t) \quad (24)$$

It is well-known that factorization cannot be exact when overall rotation is anisotropic, even when the two types of motion are statistically independent.⁵ Furthermore, a large class of functionally relevant protein dynamics involving large amplitude internal motions on the same time scale as global rotation would not be expected to be factorizable. Nevertheless, a product form for the total correlation function is often assumed in analysis of NMR relaxation data, especially in conjunction with the use of the Lipari-Szabo model free (LS-MF) approach.⁵

With this in mind, we compare the total correlation function of backbone amide NH vectors, $C_{tot}^{MD}(t)$, with product form correlation functions $C_{rot}(t)C_{int}(t)$, where the factors are given by

$$C_{rot}(t) = \langle P_l[\Omega(t) n^{LF}(0) \cdot n^{LF}(0)] \rangle \quad (25)$$

$$C_{int}(t) = \langle P_l[n^{MF}(t) \cdot n^{MF}(0)] \rangle \quad (26)$$

In eq 25, $\Omega(t)$ denotes the time-dependent Euler angle transformation that rotates the laboratory fixed (LF) reference axis system into the protein molecular frame. In the present work, $\Omega(t)$ is generated using the standard rms fitting procedure, implemented with the *ptraj* routine within the Amber 9 package. $C_{rot}(t)$ is then determined by applying $\Omega(t)$ to the NH vectors of interest at their initial LF orientation (in the reference structure). The internal correlation function, $C_{int}(t)$, is simultaneously computed with *ptraj*. In practice, we first computed the time-averaged internal structure of a protein during the trajectory and then used this average structure as the reference structure to perform the rms fits to generate both $C_{rot}(t)$ and $C_{int}(t)$.

Figure 11 shows typical internal correlation functions, which decay to plateau values with varying internal time constants; similar plots have been presented many times before.^{6,10,43,44} Many N–H vectors (such as in residues 49 in GB3 or 63 in ubiquitin) decay to constant values on a time scale of a few picoseconds, with order parameters (their asymptotic values) above 0.8. It is hardly surprising that these correlation functions factor almost perfectly. Of greater interest are floppier residues, with order parameters less than 0.8 and internal decay times that are comparable to overall tumbling times: see, for example, residue 41 in GB3, whose internal correlation function decays with a τ_e of 2.1 ns. Such slow decays have received much less attention, since they can only be reliably observed with fairly long simulations.

In Figure 12, we compare $C_{tot}^{MD}(\tau)$ with $C_{rot}(\tau)C_{int}(\tau)$ for selected backbone amide NH vectors. The product correlation

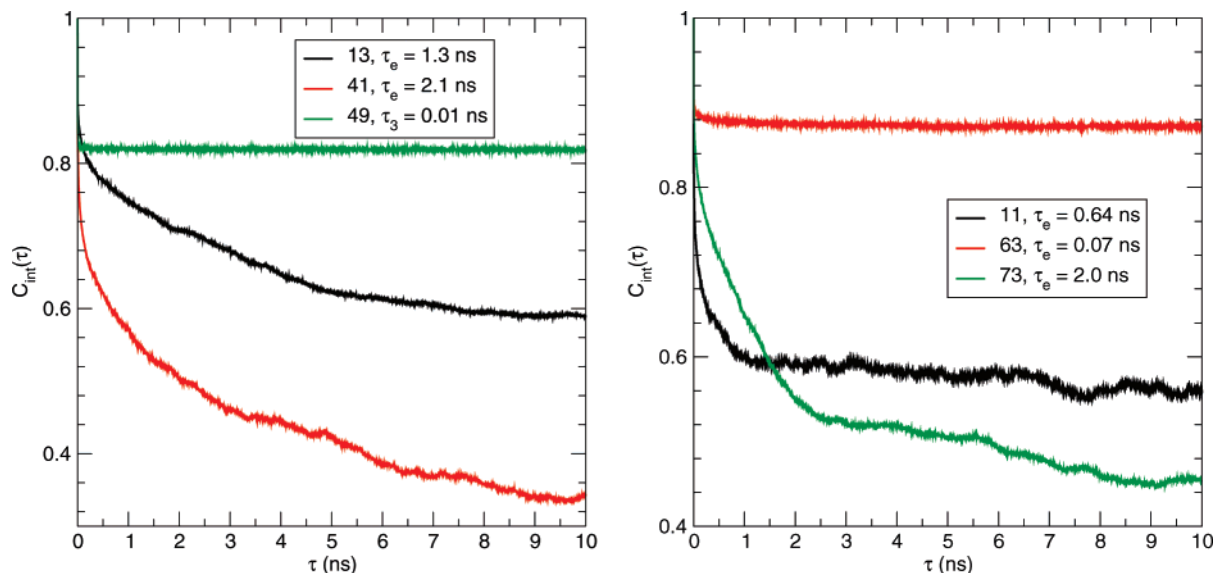


Figure 11. Internal correlation functions for selected residues in GB3 + SPC/E (left) and ubiquitin + SPC/E (right). Values of τ_e show the model-free value for the decay time of these internal correlation functions.⁵

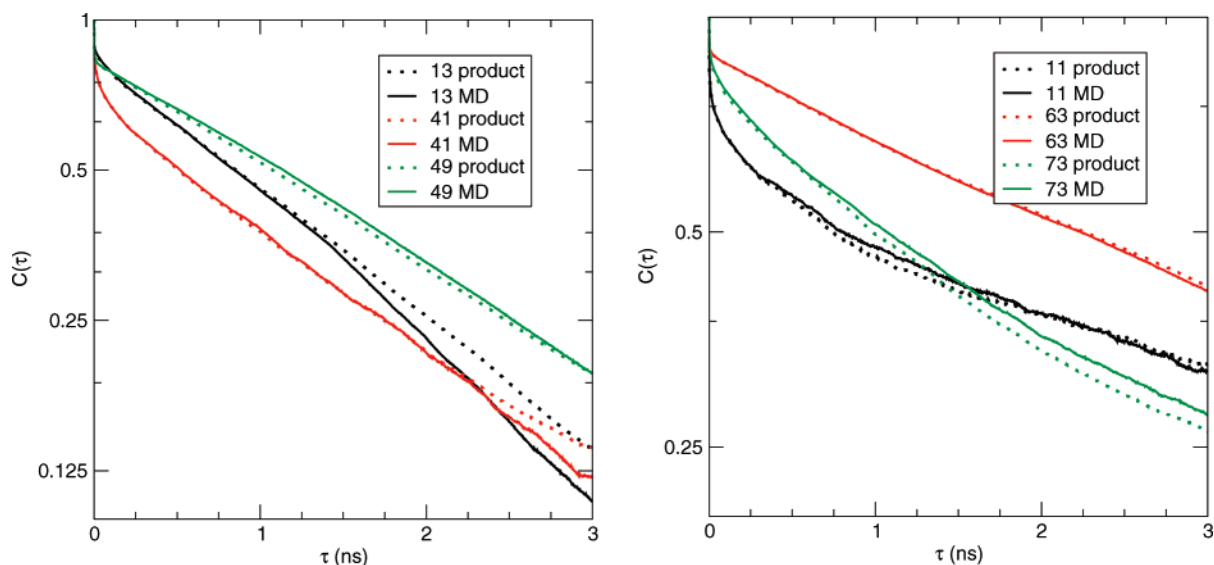


Figure 12. Comparison of selected N-H correlation functions: solid lines are computed directly from the trajectory; dashed lines represent the product $C_{\text{rot}}(\tau)C_{\text{int}}(\tau)$. Left, GB3 + SPC/E; right, ubiquitin + SPC/E.

functions are indistinguishable from the total correlation functions for delays shorter than 1 ns; small deviations beyond this are probably dominated by statistical noise in the correlation functions. For many residues, the agreement remains good for longer delays, including past lag times where the correlation functions are clearly dominated by noise. Residues in both relatively rigid secondary structure elements and those in flexible regions can be found in this category. For a small minority of residues (such as residue 13 in GB3), significant deviations of $C_{\text{rot}}(\tau)C_{\text{int}}(\tau)$ from $C_{\text{tot}}^{\text{MD}}(\tau)$ can be found for delay times between 1 and 3 ns. These are associated with floppy residues located within or near flexible loops or chain termini. In these cases, the divergences generally occur at lag times beyond which strongly nonexponential behavior is seen in the correlation function decays and for which statistical noise may dominate. Thus, for almost all residues we surveyed, agreement between the product form and the sampled total correlation functions was excellent at least up to delays where finite trajectory length may cause the correlation functions to have large uncertainties.

4. Conclusions

Molecular simulations of macromolecules offer a unique window into microscopic aspects of time-dependent phenomena, but relatively little attention has been paid to the accuracy of current force fields in describing overall motion such as rotational diffusion. Because the self-diffusion constants of popular water models like TIP3P are so much larger than experiment,⁹ it is long been suspected that protein diffusion would be too fast, and this is borne out by the current simulations. Rotational diffusion constants appear to be somewhat too large even for models like SPC/E and TIP4P/EW, whose self-diffusion constants are in better agreement with experiment. Rotational diffusion probes a sensitive balance between water–water and water–protein hydrogen-bond (and other) interactions, and work to optimize this behavior should lead to more realistic molecular simulations. It is likely that the details of hydration layer around proteins are inaccurate in all common protein–water potentials. Since the amplitudes and time scales of internal motions are likely to be coupled to overall

motion, finding potentials that give a good account of global diffusional is likely to be a prerequisite for correct simulations of internal motions as well.

We only consider here the behavior of small, well-folded proteins, whose global behavior is expected to conform to a diffusion model with a single, global diffusion tensor. The simulations for the most part bear this out, although the details of the ubiquitin simulations (in all three water models) show a dependence on the integration time τ_f that is much larger than than seen for the other proteins (see Figure 4). All of the proteins, including ubiquitin, show the expected dependence of relaxation times on $l(l+1)$, as shown in Figure 8. These studies on well-folded proteins should provide a reference point for studies of floppier systems (which are in progress), where more significant deviations from a single-diffusion-constant model are expected.

The statistical noise seen in the results in Figure 3 is somewhat discouraging, if not really unexpected. In order to follow these decays reliably, trajectories that are many times longer than the rotational correlation time are required, and these are still time consuming to compute. (As an example, a 100 ns simulation of ubiquitin with SPC/E water requires about 11 days of processing on 16 1.3 GHz Itanium processors.) The correlation functions are much better determined at short delay times, but using only short delay values runs the risk of an extrapolation error to the much longer times of actual interest and also runs the risk that breakdowns in the diffusion model might not be seen until longer delays, potentially hiding some of the most interesting results. Using l values higher than 2 leads to correlation functions that decay more rapidly, and there may be some benefit in using these to estimate diffusional behavior, again with the caveat that deviations from diffusive behavior might be missed. Many more simulations will be required for an optimal analysis scheme to become clear. It is also clear (as one would expect) that fitting the anisotropy or rhombicity of diffusion tensors requires even more extensive sampling.

Analyses of NMR relaxation data typically assume that internal motions are statistically independent from overall diffusion, at least for the types of well-folded systems studied here. Our results seem to confirm this model: even though some N-H vectors show internal decay times that are of the same order of magnitude as overall tumbling, the product approximation in eq 24 is quite well-satisfied, as shown in Figure 12. Again, future studies with floppier proteins should help to clarify the range of applicability of this sort of model.

Acknowledgment. This work was supported by NIH Grant GM45811. We thank David Fushman and Jennifer Hall for helpful discussions and for providing details of their experimental analyses.

References and Notes

- Favro, L. D. Theory of the rotational Brownian motion of a free rigid body. *Phys. Rev.* **1960**, *119*, 53.
- Berne, B.J.; Pecora, R. *Dynamic Light Scattering, with Applications to Chemistry, Biology and Physics*; Dover: Mineola, NY, 2000.
- Abraham, A. *Principles of Nuclear Magnetism*; Clarendon Press: Cambridge, 1961.
- Cavanagh, J.; Fairbrother, W. J.; Palmer, A. G., III; Rance, M.; Skelton, N. J. *Protein NMR Spectroscopy: Principles and Practice*, 2nd ed.; Academic Press: Burlington, MA, 2007.
- Lipari, G.; Szabo, A. Model-free approach to the interpretation of nuclear magnetic resonance relaxation in macromolecules. I. Theory and range of validity. *J. Am. Chem. Soc.* **1982**, *104*, 4546–4559.
- Palmer, A. G., III. NMR characterization of the dynamics of biomacromolecules. *Chem. Rev.* **2004**, *104*, 3623–3640.
- Ochsenbein, F.; Neumann, J. M.; Guittet, E.; vanHeijenoort, C. Dynamical characterization of residual and non-native structures in a partially folded protein by 15N NMR relaxation using a model based on a distribution of correlation times. *Protein Sci.* **2002**, *11*, 957–964.
- Horn, H. W.; Swope, W. C.; Pitera, J. W.; Madura, J. D.; Dick, T. J.; Hura, G. L.; Head-Gordon, T. Development of an improved four-site water model for biomolecular simulations: TIP4P-Ew. *J. Chem. Phys.* **2004**, *120*, 9665–9678.
- Mark, P.; Nilsson, L. Structure and Dynamics of the TIP3P, SPC, and SPC/E Water Models at 298 K. *J. Phys. Chem. A* **2001**, *105*, 9954–9960.
- Case, D. A. Molecular Dynamics and NMR Spin Relaxation in Proteins. *Acc. Chem. Res.* **2002**, *35*, 325–331.
- Smith, P. E.; van Gunsteren, W. F. Translational and rotational diffusion of proteins. *J. Mol. Biol.* **1994**, *236*, 629–636.
- Huntress, W. T. Effects of anisotropic molecular rotational diffusion on nuclear magnetic relaxation in liquids. *J. Chem. Phys.* **1968**, *48*, 3524–3533.
- Korzhev, D. M.; Billeter, M.; Arseniev, A. S.; Orekhov, V. Y. NMR studies of tumbling and internal motions in proteins. *Prog. Nucl. Magn. Reson. Spectrosc.* **2001**, *38*, 197–266.
- Woessner, D. E. Nuclear spin relaxation in ellipsoids undergoing rotational Brownian motion. *J. Chem. Phys.* **1962**, *37*, 647–654.
- Hubbard, P. S. Nuclear magnetic relaxation of three and four spin molecules in a liquid. *Phys. Rev.* **1958**, *109*, 1153–1158.
- Woessner, D. E. Spin-relaxation processes in a two-proton system undergoing anisotropic reorientation. *J. Chem. Phys.* **1962**, *36*, 1–4.
- Schwalbe, H.; Carlomagno, T.; Hennig, M.; Junker, J.; Reif, B.; Richter, C.; Griesinger, C. Cross-correlated relaxation for measurement of angles between tensorial interactions. *Methods Enzymol.* **2001**, *338*, 35–81.
- Brüschweiler, R.; Liao, X.; Wright, P. E. Long-range motional restrictions in a multidomain zinc-finger protein from anisotropic tumbling. *Science* **1995**, *268*, 886–889.
- Lee, L. K.; Rance, M.; Chazin, W. J.; Palmer, A. G., III. Rotational diffusion anisotropy of proteins from simultaneous analysis of ¹⁵N and ¹³C nuclear spin relaxation. *J. Biomol. NMR* **1997**, *9*, 287–298.
- Ghose, R.; Fushman, D.; Cowburn, D. Determination of rotational diffusion tensor of macromolecules in solution from NMR relaxation data with a combination of exact and approximate methods. Application to the determination of interdomain orientation in multidomain proteins. *J. Magn. Reson.* **2001**, *149*, 204–217.
- Kay, L. E.; Torchia, D. A.; Bax, A. Backbone dynamics of proteins as studied by nitrogen-15 inverse detected heteronuclear NMR spectroscopy: application to staphylococcal nuclease. *Biochemistry* **1989**, *28*, 8972–8979.
- Press, W. H.; Flannery, B. P.; Teukolsky, S. A.; Vetterling, W. T. *Numerical Recipes. The Art of Scientific Computing*; Cambridge University Press: Cambridge, U.K., 1986.
- Hall, J. B.; Fushman, D. Characterization of the overall and local dynamics of a protein with intermediate rotational anisotropy: Differentiating between conformational exchange and anisotropic diffusion in the B3 domain of protein G. *J. Biomol. NMR* **2003**, *27*, 261–275.
- Amadei, A.; Linssen, A. B. M.; Berendsen, H. J. C. Essential dynamics of proteins. *Proteins* **1993**, *17*, 412–425.
- Hünenberger, P. H.; Mark, A. W.; van Gunsteren, W. F. Fluctuation and cross-correlation analysis of protein motions observed in nanosecond molecular dynamics simulations. *J. Mol. Biol.* **1995**, *252*, 492–503.
- Karplus, M.; Ichiye, T. Comment on a “Fluctuation and cross correlation analysis of protein motions observed in nanosecond molecular dynamics simulations”. *J. Mol. Biol.* **1996**, *263*, 120–122.
- Zhou, Y.; Cook, M.; Karplus, M. Protein Motions at Zero-Total Angular Momentum: The Importance of Long-Range Correlations. *Biophys. J.* **2000**, *79*, 2902–2908.
- Theobald, D. L.; Wuttke, D. S. THESEUS: maximum likelihood superpositioning and analysis of macromolecular structures. *Bioinformatics* **2006**, *22*, 2171–2172.
- Zwanzig, R.; Ailawadi, N. K. Statistical error due to finite time averaging in computer experiments. *Phys. Rev.* **1969**, *182*, 280–283.
- Lu, C. Y.; van den Bout, D. A. Effect of finite trajectory length on the correlation function analysis of single molecule data. *J. Chem. Phys.* **2006**, *125*, 124701.
- Gronenborn, A. M.; Filpula, D. R.; Essig, N. Z.; Achari, A.; Whitlow, M.; Wingfield, P. T.; Clore, G. M. A novel, highly stable fold of the immunoglobulin binding domain of streptococcal protein G. *Science* **1991**, *253*, 657–661.
- Yakovlev, G. I.; Moiseyev, G. P.; Struminskaya, N. K.; Borzykh, O. A.; Kipenskaya, L. V.; Znamenskaya, L. V.; Leschinskaya, I. B.; Chernokalskaya, E. B.; Hartley, R. W. Mutational analysis of the active site of RNase of *Bacillus intermedius* (BINASE). *FEBS Lett.* **1994**, *354*, 305–306.
- Case, D. A.; Cheatham, T. E., III; Darden, T.; Gohlke, H.; Luo, R.; Merz, K.M., Jr.; Onufriev, A.; Simmerling, C.; Wang, B.; Woods, R. The Amber biomolecular simulation programs. *J. Comput. Chem.* **2005**, *26*, 1668–1688.

- (34) Wang, J.; Cieplak, P.; Kollman, P. A. How well does a restrained electrostatic potential (RESP) model perform in calculating conformational energies of organic and biological molecules? *J. Comput. Chem.* **2000**, *21*, 1049–1074.
- (35) Hornak, V.; Abel, R.; Okur, A.; Strockbine, B.; Roitberg, A.; Simmerling, C. Comparison of multiple Amber force fields and development of improved protein backbone parameters. *Proteins* **2006**, *65*, 712–725.
- (36) Berendsen, H. J. C.; Grigera, J. R.; Straatsma, T. P. The missing term in effective pair potentials. *J. Phys. Chem.* **1987**, *91*, 6269–6271.
- (37) Box, G. E. P.; Jenkins, G. M. *Time Series Analysis: Forecasting and Control*; Holden-Day: New York, 1976.
- (38) Brockwell, P. J.; Davis, R. A. *Time Series: Theory and Methods*; Springer-Verlag: New York, 1991.
- (39) Tjandra, N.; Feller, S. E.; Pastor, R. W.; Bax, A. Rotational diffusion anisotropy of human ubiquitin of ^{15}N NMR relaxation. *J. Am. Chem. Soc.* **1995**, *117*, 12562–12566.
- (40) Wang, T.; Cai, S.; Zuiderweg, E. R. P. Temperature Dependence of Anisotropic Protein Backbone Dynamics. *J. Am. Chem. Soc.* **2003**, *125*, 8639–8643.
- (41) Buck, M.; Boyd, J.; Redfield, C.; MacKenzie, D. A.; Jeenes, D. J.; Archer, D. B.; Dobson, C. M. Structural determinants of protein dynamics: Analysis of ^{15}N NMR relaxation measurements for main-chain and side-chain nuclei of hen egg white lysozyme. *Biochemistry* **1995**, *34*, 4041–4055.
- (42) Weast, R. C. *CRC Handbook of Chemistry and Physics*, 59th ed.; CRC Press: West Palm Beach, FL, 1978.
- (43) Lipari, G.; Szabo, A.; Levy, R. M. Protein dynamics and NMR relaxation: comparison of simulations with experiment. *Nature* **1982**, *300*, 197–198.
- (44) Palmer, A. G.; Case, D. A. Molecular dynamics analysis of NMR relaxation in a zinc-finger peptide. *J. Am. Chem. Soc.* **1992**, *114*, 9059–9067.